Barcelona '10

F020

Fault Activation During Hydraulic Fracturing

S.C. Maxwell* (Schlumberger Canada), M. Jones (Schlumberger Canada), R. Parker (Schlumberger Canada), S. Leaney (Schlumberger), M. Mack (Schlumberger), D. Dorvall (Talisman), D. D'Amico (Talisman), J. Logel (Talisman), E. Anderson (Talisman) & K. Hammermaster (Talisman)

SUMMARY

Microseismic imaging was used to image hydraulic fracturing during a gas well stimulation. Some time after the end of the injection, there was an increase in the seismic deformation rate. Investigation of the frequency-magnitude characteristics during the pumping were consistent with other hydraulic fracture results, although the activity recorded after the end of pumping was more consistent with observations of natural seismic deformation along faults. The ratio of p- to s-wave amplitudes also varied for events recorded during the pumping compared to those occurring after the end of pumping, suggesting a different failure mechanism. In this example, it appears that the hydraulic fracture induced movement on a nearby fault. Geomechanical modeling was also performed to examine induced stresses associated with the stimulation, and investigate possible fault deformation.

Introduction

Microseismic imaging is a powerful method to map the hydraulic fracture stimulation of a well. Often the spatial-temporal location of induced microseisms is used to image the dynamics of the fracture growth, allowing optimization of the stimulation to maximum reservoir contact. Beyond the hypocentral locations of the microseisms, additional attributes of the microseisms can also be used to improve the imaging of the geomechanical deformation and help refine the interpretation of a fracture network (eg. Maxwell et al, 2007).

In this paper, we present results of the monitoring a hydraulic fracture with sensors in two observation wells. The spatial distribution of the microseisms is first presented to illustrate the fracture. The temporal evolution, strength of the microseisms, frequency-magnitude relationship and finally seismic phase amplitude ratios are then presented to highlight the fact that the stimulation appears to have induced deformation on a near by fault.

Microseismic Image

Microseismicity was used to image a hydraulic fracture stimulation of a gas well in Western Canada. The well intersected a reverse fault system (Figure 1) with low angle thrust faults ranging in dip from 20-30°. Throw along the faults averages 30m (Figure 2). Sandstones of the formation were deposited in a prograding shoreface system and are composed of lower to upper shoreface sands. Sands are regionally massive, reworked and continuous through out the area. Upper fine to medium sized grained quartz cemented sandstones with silica overgrowths occluding primary porosity dominate the formation. The formation is bound on either side by mudstones and very fine grained interbedded siltstones and burrowed shales that were deposited in an offshore transition environment.

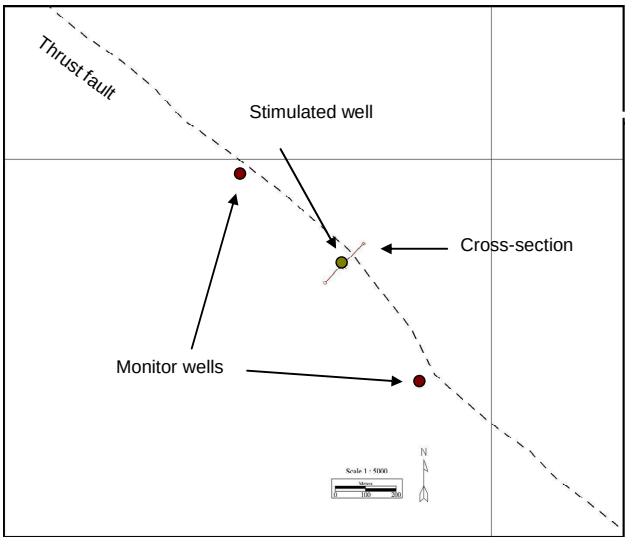

Figure 1 *Map showing trace of the fault, and orientation of cross-section in Figure 2.*

Figure 3 shows the location of induced microseisms recording during the hydraulic fracture stimulation of the gas well. The seismic events define a fairly simple fracture oriented approximately N45E. Two discrete clusters of events are observed, one extending about 100 m around the perforations, and a second cluster about 150 m to the NE. In depth, the event locations cluster close to the depth interval of the open perforations.

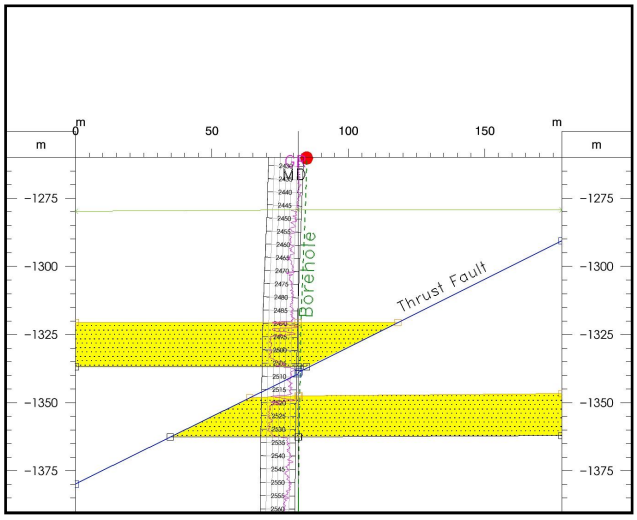

Figure 2 *Geometry of over-thrusted sands that were intersected twice with the vertical treatment well. The hydraulic fracture stimulation treated both sands simultaneously.*

Figure 4 shows a time-line of the injection pressure and rate of the hydraulic fracture stimulation, which lasted approximately 80 minutes. During the stimulation, the cumulative seismic moment slowly increased. For each of the microseisms, the source strength was computed as a seismic moment, the log of

which is defined as a moment magnitude (conceptually similar to the common Richter scale). The cumulative seismic moment curve in Figure 4 is a plot of the total seismic deformation that occurred up to a specific time. Typically, after the end of the injection, the seismic moment curve levels off as the microseismic activity rate and strength diminishes. In this example, however, the incremental seismic deformation begins to diminish after the end of pumping, but at about 140 minutes after the start of the injection the seismic deformation rapidly increases. After this increase, the seismic deformation stabilizes after about 170 minutes.

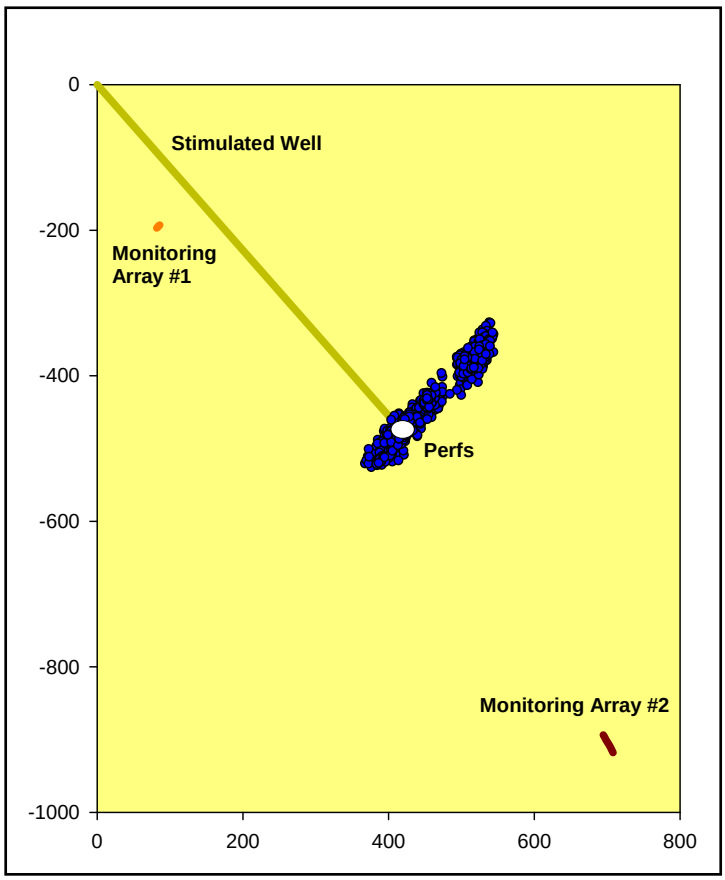

Figure 3 *Map of the microseisms recorded during a hydraulic stimulation.*

Frequency-Magnitude Relationship

Microsiesmic activity recorded during a hydraulic fracture generally follows a power law distribution described by the Gutenberg-Richter relationship:

$$\log N = \boldsymbol{a} - \boldsymbol{b}M,$$

where N is the number of events with magnitude greater than or equal to a magnitude M and ***a*** and ***b*** are constants. The ***b***-value describing the slope of the relationship is typically around a value of 1 for natural earthquakes sequences on faults, but typically closer to a value of 2 for seismicity induced by hydraulic fracturing.

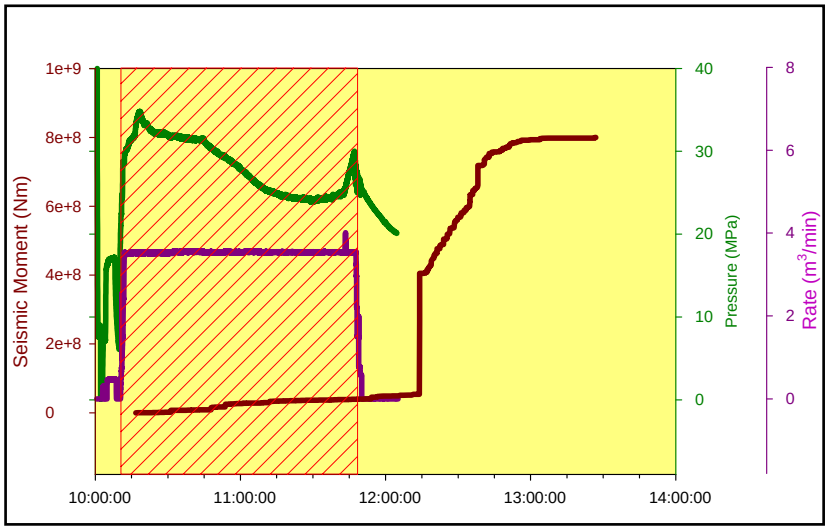

Figure 4 *Injection pressure and rate, and cumulative seismic moment indicating the total strength of the microseismic activity.*

Figure 5 shows a plot of the magnitude and frequency of events recorded during and after the frac. During the frac, the ***b***-value is approximately 2 compared to a value of less than 1 for the events after the frac. This may indicate that the period of rapid seismic deformation that occurred after the end of pumping may be associated with fault activation induced by the fracture stimulation. Regardless, the difference in the number of events at various sizes is indicative of a change in the mode of deformation.

Amplitude Ratios

The post injection microseismicity also shows a change in the ratio of p- to s-wave amplitudes. Figure 6 shows the P/S amplitude ratio for nearly horizontal raypaths recorded on array #2. Note the increase in the amplitude ratio for the post pumping fracs. As indicated above, the post frac events are spatially located to the NE compared to the pumping events that locate closer to the treatment well. Depending on the orientation of the failure planes and the characteristics of the coseismic deformation, there will be a specific directional radiation of p- and s-wave energy that results in a directional dependence of the amplitude ratios. Although not presented here for the sake of brevity, the activity recorded during and after the frac has unique radiation characteristics suggesting a different failure mechanism for the two time periods. Since the microseisms are recorded with sensors in two different observation wells, the radiation characteristics are adequately sampled for a moment tensor analysis of the deformation.

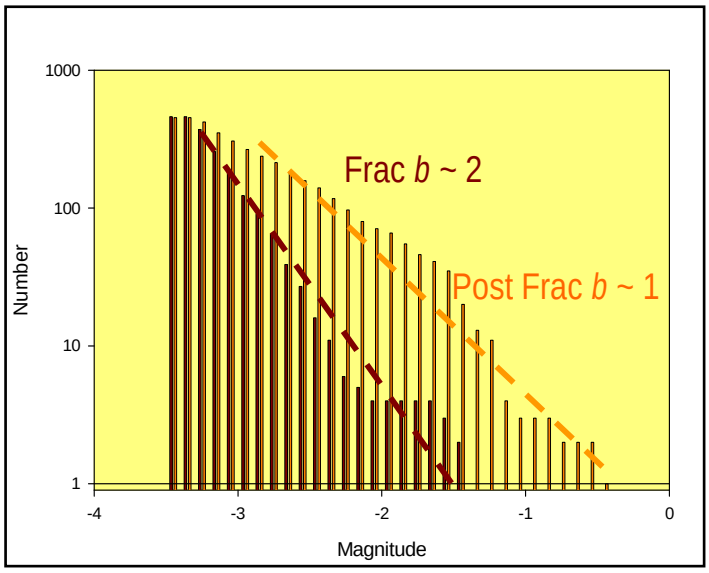

Figure 5 *Frequency-magnitude relationship of the microseisms recorded during the frac (red) compared to after the frac (orange).*

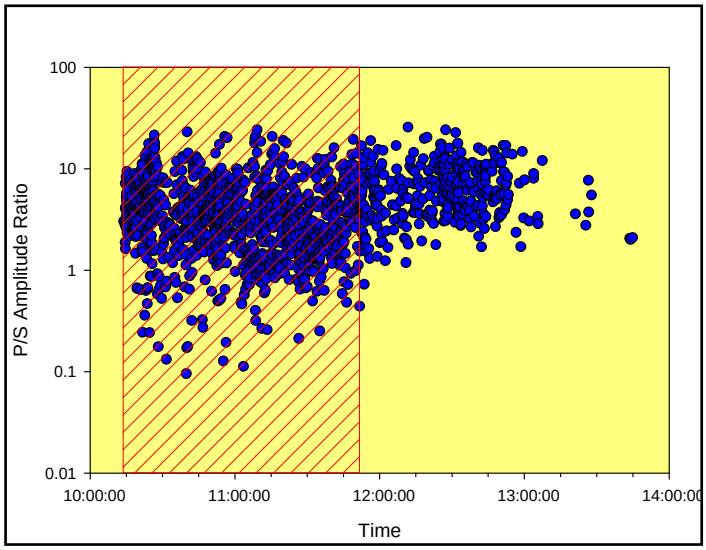

Figure 6 *Ratio of p to s-wave amplitudes recorded for nearly horizontal raypaths on array #2. Red hatched region indicates injection period.*

Geomechanics

In order to better understand how the hydraulic fracturing could influence a fault, geomechanical modeling was performed. Induced stresses and increased pore pressure associated with the hydraulic fracture were investigated to access the impact on fault deformation. Preliminary investigations suggest that the hydraulic fracture could indeed activate movement on a fault. Ongoing investigation is considering how the relative location and geometry of the fault impacts whether or not it is stable.

Conclusions

In summary, this particular hydraulic fracture appeared to result in a relatively simple fracture geometry extending in a NE-SW direction. However, after the end of pumping an increase in the seismic deformation rate occurred. These microseisms recorded after the end of pumping had a relatively low slope for the corresponding frequency-magnitude relation more consistent with natural earthquakes along a fault then typical hydraulic fracture values observed during the pumping. Spatially, the events are clustered to the NE of the treatment well in an area where few microseisms occurred during the frac. Finally, the P/S amplitude ratio of these post pumping events are relatively high compared to the events recorded during the pumping, suggesting deformation occurring in a different orientation. The implication of these observations is that the hydraulic fracture stimulation induced deformation on a nearby fault, as confirmed by geomechanical modeling. This example can serve as a basis to develop interpretational techniques to distinguish microseismicity associated with hydraulic fracturing from that associated with faulting, for a better evaluation of the stimulated rock volume.

References

Maxwell, S., U. Zimmer, R. Gusek and D. Quirk, 2007, "Imaging Hydraulic Fracture Reorientation Across a Thrust Fault", presented at 77th SEG Annual Meeting, San Antonio, Texas.